IOP PUBLISHING JOURNAL OF PHYSICS D: APPLIED PHYSICS

J. Phys. D: Appl. Phys. **41** (2008) 185202 (9pp) doi:10.1088/0022-3727/41/18/185202

Comparison between fluid simulations and experiments in inductively coupled argon/chlorine plasmas

C S Corr[1], E Despiau-Pujo[2], P Chabert[2], W G Graham[3], F G Marro[3] and D B Graves[4]

[1] Space Plasma, Power and Propulsion Group, The Australian National University, Canberra 0200, Australia
[2] Laboratoire de Physique et Technologie des Plasmas, Ecole Polytechnique, 91128, Palaiseau Cedex, France
[3] School of Mathematics and Physics, The Queen's University Belfast, Belfast BT7 1NN, Northern Ireland
[4] Department of Chemical Engineering, University of California, Berkeley, CA 94720, USA

E-mail: despiau@lptp.polytechnique.fr

Received 24 June 2008, in final form 27 July 2008
Published 28 August 2008
Online at stacks.iop.org/JPhysD/41/185202

Abstract
Comparisons of 2D fluid simulations with experimental measurements of Ar/Cl_2 plasmas in a low-pressure inductively coupled reactor are reported. Simulations show that the wall recombination coefficient of Cl atom (γ) is a crucial parameter of the model and that neutral densities are very sensitive to its variations. The best agreement between model and experiment is obtained for $\gamma = 0.02$, which is much lower than the value predicted for stainless steel walls ($\gamma = 0.6$). This is consistent with reactor wall contaminations classically observed in such discharges. The electron density, negative ion fraction and Cl atom density have been investigated under various conditions of chlorine and argon concentrations, gas pressure and applied rf input power. The plasma electronegativity decreases with rf power and increases with chlorine concentration. At high pressure, the power absorption and distribution of charged particles become more localized below the quartz window. Although the experimental trends are well reproduced by the simulations, the calculated charged particle densities are systematically overestimated by a factor of 3–5. The reasons for this discrepancy are discussed in the paper.

1. Introduction

Plasma processing is widely used to modify surfaces in thin film device manufacturing industries. III–V compounds such as GaAs, InP or GaN-based materials are increasingly important for their use in optoelectronic applications, especially in the telecommunications and light detection industries. Photonic devices, including lasers, photodetectors or light emitting diodes, require reliable etching processes characterized by high etch rate, profile control and low damage. Although many problems remain to be understood, inductively coupled discharges seem to be very promising to etch such materials, using Cl_2/Ar, Cl_2/N_2 and Cl_2/H_2 gas chemistries [1, 2]. In the microelectronics industry, low-pressure chlorine-based plasmas are also used in sub-micrometre device fabrication involving silicon and polycrystalline silicon (poly-Si) [3, 4]. Inductively coupled plasma (ICP) sources meet most of the requirements for efficient plasma processing such as high etch rates, high ion densities and low controllable ion energies [5]. However, the use of gas mixtures incorporating both electropositive and electronegative gases complicates the plasma kinetics significantly. In particular, the presence of a negative ion population in the plasma alters the positive ion flux, reduces the electron density, changes the electron temperature, modifies the spatial structure of the discharge and can cause unstable operation [6–15].

Several experimental studies and numerical simulation results have been published on inductively coupled Cl_2/Ar

plasmas [16–19], but relatively few systematic comparisons of models' predictions and experimental data have been reported in given reactor geometries, under a wide range of operating conditions. Validation of numerical predictions is essential for chemically complex plasma processing and there is a need to benchmark the models with as many measurements as possible. Consequently, in this paper, we investigate a Cl_2/Ar inductively coupled discharge and confront experimental measurements with 2D fluid model predictions of various plasma parameters and neutral quantities.

The paper is organized as follows. Section 2 describes the experimental setup and the different plasma diagnostics, based on Langmuir probe measurements, laser induced fluorescence (LIF) and photodetachment techniques. Section 3 presents the characteristics of the 2D fluid simulation of the ICP discharge, the numerical tools and the model chemistry. The effects of power, pressure and Ar/Cl_2 ratio on the chlorine atom density, the negative ion fraction and the electron density are presented and discussed in sections 2 and 3. Our conclusions are given in section 4.

2. Experimental arrangement and diagnostics

2.1. The ICP system

The experimental measurements were carried out in an ICP operating with argon and chlorine as the feed gases. The reactor has been described elsewhere [15, 20]. Briefly, the upper antenna is a planar 6-turn water-cooled coil made from a 6 mm diameter copper tube that couples power to the plasma through a 21 mm thick quartz window (200 mm diameter). The lower, 200 mm diameter, stainless steel electrode and the stainless steel vacuum vessel were grounded. The gap between the quartz window and the bottom stainless steel electrode is 85 mm. The central connection of the antenna is powered by a 13.56 MHz rf power supply through a close coupled L-type matching network. The outer connection of the coil is grounded. For all the measurements reported here the matching capacitors were adjusted to minimize the reflected power. The reported input power is the difference between the forward and averaged reflected power as read from the power supply meter. The plasma chamber was evacuated by a turbo molecular pump, which routinely achieved base pressures of 2×10^{-6} Torr. During plasma operation, the pressure was monitored by a 0–100 mTorr capacitance manometer. A four-channel MKS flow controller varied the flows of argon and chlorine into the chamber. This allowed for different gas ratios to be obtained. The total gas flow was kept constant at 10 sccm for all measurements. The pumping was throttled to maintain the desired gas pressures. All the present measurements were with gas pressures and input powers in the range from 1 to 50 mTorr and up to 400 W, respectively.

2.2. Plasma diagnostics

2.2.1. Langmuir probe. A passively compensated Langmuir probe [21, 22] was used to determine the plasma parameters from measurements of the probe $I(V)$ characteristics described previously. The electron energy probability functions (EEPF) were determined from the second derivative of the $I(V)$ characteristics [23]. The electron density and electron temperature were determined from the EEPF and the positive ion density was calculated from both the ion saturation current [24] and from the quasineutrality relation $n_+ = n_e + n_-$, where n_- was determined from the photodetachment method described below. Good agreement was found between both methods. The compensated Langmuir probe design is similar to that described previously [14, 22]. The probe tip was made from 0.125 or 0.08 mm diameter platinum wire with 10 mm extended beyond the surrounding alumina insulator. The compensated probe system consisted of the measurement probe and a separate floating reference probe to correct for fluctuations in the direct current value of the plasma potential caused by the different potentials applied to the measurement probe. Due to contamination of the probe tip when operating with discharges containing chlorine gas, the probes were cleaned after every single measurement by switching to a pure argon discharge and drawing an electron current sufficient to have the tip glow bright red. A set of benchmark time-averaged plasma parameters measurements at specific plasma operating conditions were used to determine reproducibility and to check for any longer term drifts in the plasma or measurement techniques. The plasma density could vary by a factor of 3 depending on the prior operating history of the discharge. Prior to all experimental runs, a pure argon discharge was run for about 1 h so that the chamber surfaces reached a steady-state temperature before measurements were made. The error bars presented in this paper were determined from the reproducibility of the experimental measurements when operating with the discharge at different times under the same conditions (input power, pressure and gas flow).

2.2.2. Probe-based laser photodetachment. A probe-based laser photodetachment technique, as described in [14], was used to measure the negative ion density. Briefly, the negative ion density was determined from measurements of the dc electron current (I_{dc}^-) in the absence of the laser pulse and the increase in the current (ΔI^-) immediately after the pulse using the relationship [25, 26]:

$$\frac{\Delta I^-}{I_{dc}^-} = \frac{\Delta n_e}{n_e} = \frac{n_-}{n_e} = \alpha, \tag{1}$$

where n_e and n_- are the electron and negative ion densities, respectively. The electron density is determined by the Langmuir probe measurement as discussed earlier.

For negative ion detection, the experimental arrangement consisted of a 5 mm diameter cylindrical beam, from a frequency quadrupled Nd : YAG laser (266 nm), aligned to be co-linear with an uncompensated 0.5 mm diameter platinum wire probe biased positively to detect the electrons photodetached from the negative ions. The necessary conditions for probe voltage and laser beam power conditions were determined to ensure that the negative ion fraction was measured correctly. The laser photon energy (4.65 eV) was sufficient to photodetach Cl^-, which is the dominant negative ion and has an electron affinity of 3.6 eV [27, 28]. The negative

ion species Cl_2^- will also be photodetached as the energy required is 2.5 eV. The laser beam energy dependence of the probe signal indicated that, as previously found in an inductively coupled chlorine discharge [29], Cl^- was the dominant negative ion. This measurement also indicated that at the full energy output of the laser only 75% of the negative ions in the laser beam volume were being detached. The laser energy was therefore monitored closely and the signal corrected using the calculated dependence based on the known photodetachment cross section.

2.2.3. Laser induced fluorescence (LIF). The LIF scheme used here to measure the absolute atomic chlorine density has been described elsewhere [20]. Two photons at 233.3 nm were generated using a frequency-doubled Nd : YAG laser pumped dye laser system. The dye laser was frequency doubled to produce a 597 nm beam and then frequency mixed with the remaining Nd : YAG fundamental to generate ≈3 mJ per 10 ns pulse of the desired 233.3 nm output. The laser output was focused using a 50 cm focal length quartz lens through a quartz window into the plasma centre region and 2–3 cm above the stainless steel bottom electrode. An Andor ISTAR intensified CCD camera was used to detect the LIF signal. An Oriel interference filter (central wavelength 726.92 nm, bandwidth 7.59 nm) was used to discriminate plasma emission at wavelengths other than the fluorescence signal. To obtain the absolute density, the LIF measurements were calibrated by detecting the signal from a known number of chlorine atoms. Here, the plasma chamber was filled to a known pressure with CCl_4 and identical measurements were made to those in the plasma discharges. A known density of chlorine atoms is produced by the photo-dissociation of CCl_4 [30]. This molecule also has a quantum yield of almost unity for CCl_3 production at wavelengths greater than 230 nm, indicating that the photolysis of the molecule into CCl_3 and a Cl radical is the dominant photo-dissociation process.

3. Model of the ICP discharge

In this work, a 2D fluid model, initially developed by Hsu *et al* [31], is used to investigate Cl_2/Ar chemistries and study the influence of various operating conditions on both plasma and neutrals characteristics. This model is able to calculate plasma parameters within the reactor volume, along with neutral radical densities and profiles for purely inductive discharges. In this paper, only a brief description of the model is given but more details on the computational procedures and the equation set can be found elsewhere [31].

3.1. Model formulation

This model couples plasma electrodynamics to neutral chemistry and transport. Electrons, ions and neutrals are treated as three continuum fluids with exchange of mass, momentum and energy through appropriate source and loss terms. The plasma is assumed to be ambipolar and quasineutral. The drift–diffusion approximation is applied for ions and electron fluxes. Ions are assumed to be

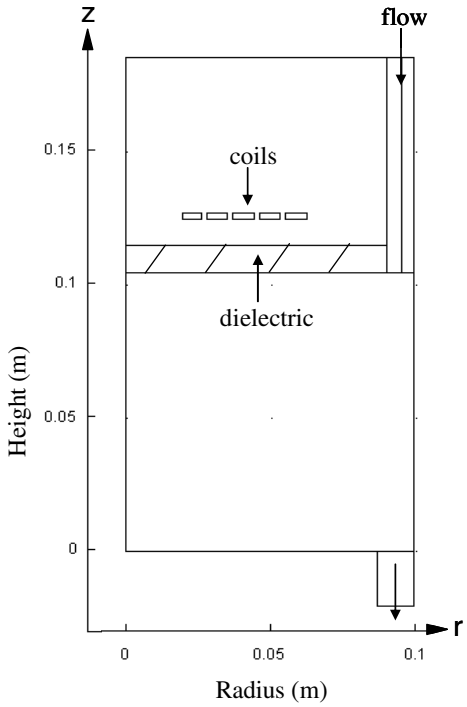

Figure 1. The model geometry of the ICP reactor.

isothermal with $T_i = 0.05$ eV and ion inertia is neglected. A key assumption of the model is the Maxwell–Boltzmann electron energy distribution function (EEDF). Assuming quasineutrality, the electron density (n_e) is set equal to the sum of positive ion densities minus negative ion densities. Since Poisson's equation is not solved, the model does not include the sheath dynamics. The neutral species are assumed to be in local thermal equilibrium characterized by a single temperature, therefore we solve a single energy balance equation for the neutral gas. Power deposited into electrons comes from inductive coupling from an external coil. The current version of the model is intended to obtain steady-state solutions.

The model geometry and the set of equations are set up and solved using the coupled COMSOL–MATLAB platforms. The potential advantages of using these commercial packages include improved standardization, portability and transparency, as well as the possibility to easily modify the geometry. In this paper, the model reactor was designed to match the geometry and the dimensions of the experimental ICP setup, as shown in figure 1. The system is predominantly cylindrical and perfectly axially symmetric, with a 20 cm diameter and 10 cm long plasma chamber. Interior walls are assumed to be grounded (stainless steel) and the top surface dielectric (quartz window). The wall temperature floats in practice but is generally ≈40°C and is assumed to be room temperature in the model. The gas flow arrives from the top annular region and is removed through the radial annular edges at the bottom. Simulations are generally run between 5–100 mTorr, 0–100 sccm and 50–1000 W.

Eight different species are included in the model, as listed in table 1. Ar, Cl and Cl_2 electronic excitations to metastable or resonant states are included in the electron energy loss channel, but only ground electronic state densities are

Table 1. Species included in the model.

e, Ar, Ar^+, Cl_2, Cl_2^+, Cl, Cl^+, Cl^-

Table 2. Volume reactions included in the model.

Label	Process	References
Electron impact		
1	$e + Ar \rightarrow Ar^+ + 2e$	[32]
2	$e + Ar \rightarrow Ar^m + e$	[32]
3	$e + Ar \rightarrow Ar^* + e$	[32]
4	$e + Cl_2 \rightarrow Cl_2^+ + 2e$	[33]
5	$e + Cl_2 \rightarrow 2Cl + e$	[33]
6	$e + Cl_2 \rightarrow Cl^+ + Cl^- + e$	[33]
7	$e + Cl_2 \rightarrow Cl + Cl^-$	[33]
8	$e + Cl_2 \rightarrow Cl^+ + Cl + 2e$	[33]
9	$e + Cl_2 \rightarrow Cl_2(b\,^3\Pi_u) + e$	[33]
10	$e + Cl_2 \rightarrow Cl_2(^1\Pi_u) + e$	[33]
11	$e + Cl_2 \rightarrow Cl_2(^1\Pi_g) + e$	[33]
12	$e + Cl_2 \rightarrow Cl_2(^1\Sigma_g) + e$	[33]
13	$e + Cl_2 \rightarrow Cl_2(Ryd) + e$	[34]
14	$e + Cl \rightarrow Cl^+ + 2e$	[33]
15	$e + Cl \rightarrow Cl(^3D) + e$	[33]
16	$e + Cl \rightarrow Cl(^4D) + e$	[33]
17	$e + Cl \rightarrow Cl(^4P) + e$	[33]
18	$e + Cl \rightarrow Cl(^4S) + e$	[33]
19	$e + Cl \rightarrow Cl(^5D) + e$	[33]
20	$e + Cl \rightarrow Cl(^5P) + e$	[33]
21	$e + Cl^- \rightarrow Cl + 2e$	[33]
Charge exchange		
22	$Cl_2 + Ar^+ \rightarrow Cl_2^+ + Ar$	[a]
23	$Cl + Ar^+ \rightarrow Cl^+ + Ar$	[b]
Neutralization		
24	$Cl^- + Cl_2^+ \rightarrow Cl + Cl_2$	[35]
25	$Cl^- + Cl^+ \rightarrow 2Cl$	[35]

[a] Estimated to be the same as the Ar^+/O_2 reaction from [33].
[b] Estimated to be the same as the Ar^+/O_2 reaction from [33].

followed. The inelastic electron impact reactions as well as the charge exchange and neutralization reactions are listed in table 2. For each species, the net neutral flux at the walls is the sum of the fluxes for radical recombination and ion neutralization. Wall chemistry is described in a relatively simple way, employing overall reaction coefficients rather than a site balance model.

3.2. Remarks and improvements

The expression for the electron energy flux at the walls into the electron energy equation was modified, in order to take into account the potential drop within the sheath between the plasma and the floating walls. In the presence of the sheath, the electron flux at the walls is [5]:

$$\Gamma_e = \frac{1}{4} n_s \bar{v_e} \exp\left(\frac{\Phi_w}{kT_e}\right), \tag{2}$$

where v_e is the mean electron speed and Φ_w is the potential of the wall with respect to the sheath–presheath edge. And the electron energy flux at the walls is

$$Q_e = 2kT_e\Gamma_e\left(1 + \frac{e\Phi_w}{2kT_e}\right). \tag{3}$$

So if the space charge sheath is considered, the kinetic energy loss at the walls increases. By assuming $\Phi_w \approx 5kT_e$, we obtain $Q_e = 7kT_e\Gamma_e$. Using this expression instead of $2kT_e\Gamma_e$ makes n_e decrease by ≈25%.

The expression of the ion flux at the walls was also modified. Initially, the radial centreline had zero flux and at the walls, the ion flux was set equal to the Bohm flux:

$$\Gamma_{j^+} = n_{j^+} * \sqrt{\frac{eT_e}{M_j}}, \tag{4}$$

where n_{j^+} is the density of positive ion j at the wall, and $\sqrt{eT_e/M_j}$ the Bohm velocity. However, when the electronegativity is large (typically larger than 2), this boundary expression must be modified with the following velocity condition [5]:

$$u_s \geqslant \left[\frac{eT_e(1+\alpha_s)}{M(1+\alpha_s\gamma)}\right]^{\frac{1}{2}}, \tag{5}$$

where M is the positive ion mass, $\gamma \equiv T_e/T_-$ and α_s is the electronegativity at the sheath edge. When α_s is large, the expression becomes

$$u_s \geqslant \left[\frac{eT_-}{M}\right]^{\frac{1}{2}}. \tag{6}$$

At low electronegativity, the plasma tends to stratify into an electronegative core and an electropositive edge, and the Bohm criterion is not modified. Note that this stratification occurs because the ambipolar field required to confine the mobile electrons pushes the negative ions into the discharge centre. In the high electronegative regime, the electron density becomes uniform, the negative ions fill the entire discharge volume and the Bohm velocity is modified [5]. For the discharge conditions simulated in this paper, the negative ion fraction rarely exceeds 2.5, and therefore, the electropositive expression of the Bohm velocity was often a good approximation. However, the effect of the modified Bohm velocity proved very important in other regimes explored but not presented in this paper.

Another important parameter in the model is the assumed fraction of the ICP power deposited into electrons. The net power into the plasma was estimated experimentally by measuring power losses into the external circuit and matching network with the plasma off. It was observed that transmission efficiency is much better in inductive operation and varies with gas chemistry. For instance, this efficiency was estimated to be around 20–40% in capacitive mode and 70–80% in inductive mode, depending on the pressure and gas mixture. We used these results to scale the power in the model such that the value used in the simulations is actually a fraction of the total delivered power.

Finally, the recombination probability of the Cl radical on the reactor walls was also modified. In the model, the neutral flux of Cl_2 at the walls due to recombination is given by

$$\Gamma_{Rec,Cl_2} = \frac{1}{4}\left(\frac{\gamma}{1-\gamma/2}\right) * w_{Cl} * \rho * \bar{v_{Cl}}, \tag{7}$$

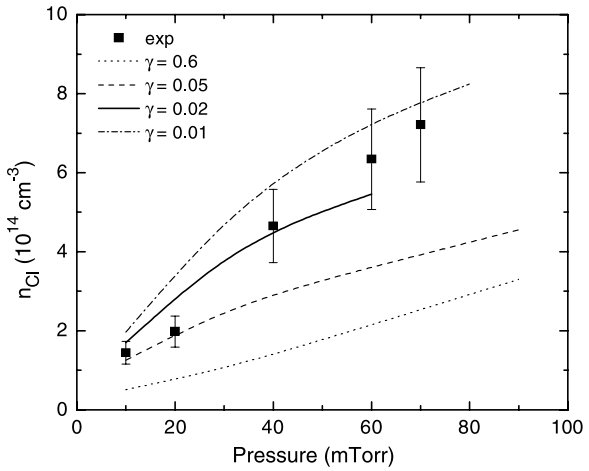

Figure 2. The atomic chlorine dependence on pressure for a pure chlorine plasma at 400 W. The dots represent experimental data while lines represent modelling results, for various wall recombination coefficients of Cl atom.

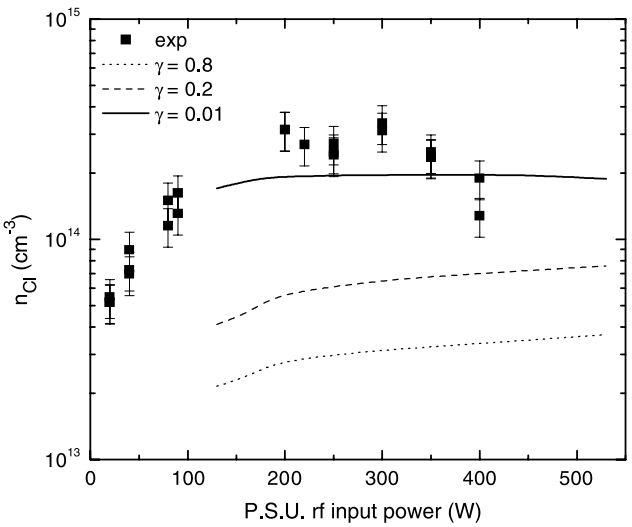

Figure 3. The atomic chlorine dependence on power for a pure chlorine plasma at 10 mTorr. The dots represent experimental data while lines represent modelling results, for various wall recombination coefficients of Cl atom.

where γ, w, ρ and $\bar{v}$ are, respectively, the surface recombination coefficient, mass fraction, mass density and thermal velocity of the Cl radical. The initial recombination coefficient was taken from Kota *et al* [36], assuming $\gamma = 0.6$ for stainless steel walls and $\gamma = 0.05$ for the quartz window. However, it was noted that varying γ had a big influence on expression (7) and greatly modified the neutral densities. Figure 2 shows the measured pressure dependence of the chlorine atom density at 400 W as well as the model predictions for different values of the recombination coefficient. In inductive mode, we observe that the atomic chlorine density increases with increasing pressure, reaching 7.21×10^{14} cm^{-3} at 70 mTorr. The model predictions show that γ must be between 0.05 and 0.01 to quantitatively fit the experimental data, which is much lower than 0.6. However, since there was no plasma cleaning of the chamber walls during the experimental campaign, we believe that deposition of films on stainless steel surfaces could modify the recombination probability of Cl radicals. Contaminants on the wall were not analysed, however, Cunge *et al* showed that chlorine plasmas operated in reactors of different wall coatings, under otherwise identical plasma conditions, have completely different Cl mole fractions because the recombination probability of Cl atoms is strongly surface dependent [37]. For instance, they showed that the recombination coefficient of Cl atoms can be 0.005 on SiOCl film while it is about 0.3 on AlF, CCl or TiOCl coated reactors. Also, the recombination coefficients were measured to be fairly strong functions of surface temperature and to drop pretty rapidly above 300 K [36]. Figure 3 displays the chlorine atom density as a function of input power at 10 mTorr for a pure chlorine plasma, for both experiment and model. The experimentally measured chlorine atom density displays a maximum of 3×10^{14} cm^{-3} at 200 W, remains constant up to 300 W and then decreases at higher powers probably because of gas heating [20]. Here the trends predicted by the model agree well with the experiment for $\gamma = 0.01$, even if we do not observe a pronounced decay of Cl density at high powers. In any case, these figures show that n_{Cl} is strongly dependent on the recombination coefficient and that the best agreement between model and experiment is obtained for low values of γ, therefore, we decided to take $\gamma = 0.02$ for all our simulations.

4. Results and discussion

We start our discussion by examining the EEPF, which plays a very important role in the plasma since it governs all the inelastic electron impact processes. The EEPFs for various argon–chlorine plasmas at 10 mTorr and 200 W are shown in figure 4. In the experimental system, the EEPF changes from a truncated Maxwellian in a pure argon plasma to a single Maxwellian in a pure chlorine plasma. This phenomenon is due to the increase in inelastic collisions with higher threshold energies in argon, in comparison with chlorine, which depletes the EEPF. As the chlorine flow increases, these processes are removed, resulting in the single Maxwellian profile. For 50% chlorine concentration, the EEPF becomes Maxwellian for input powers greater than 150 W. In pure chlorine, it occurs at higher power ($\geqslant$200 W). Consequently, as observed experimentally, the assumption of a Maxwellian EEPF in our model treatment of electrons is a good approximation for Ar/Cl_2 mixtures in inductive mode.

4.1. Power dependence

Figure 5 displays the electron density dependence on power at 10 mTorr, for both the experiment and the model. Contrary to the GEC inductively coupled reactor [14], this particular system does not show a sudden transition from the E to the H mode with increasing power, usually characterized by a pronounced increase in density and light intensity. However, the switch from the capacitive to the more efficient inductive mode can be observed at defined input powers, being $\approx$80 W in pure argon and moving to higher values with increasing chlorine concentration. The model does not include any

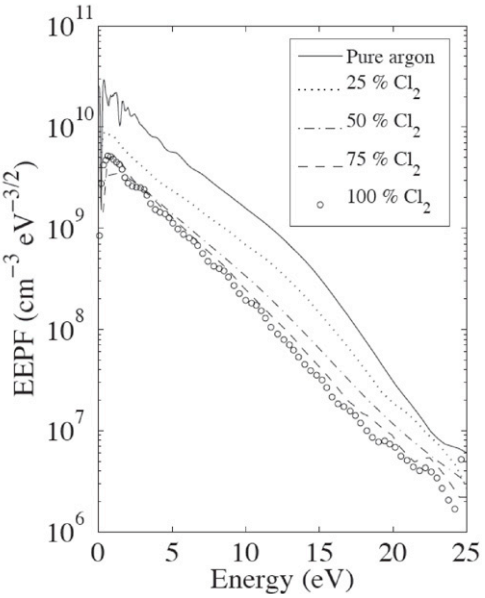

Figure 4. EEPF for various concentrations of argon and chlorine at 10 mTorr and 200 W.

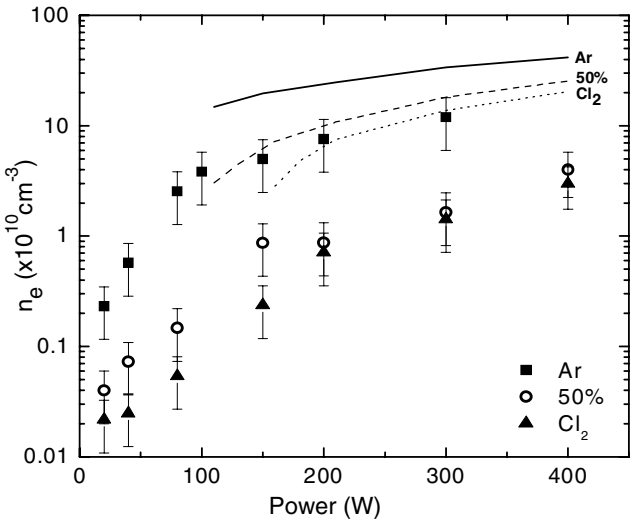

Figure 5. The electron density dependence on power at 10 mTorr, for various chlorine concentrations. Dots represent experimental data while lines represent modelling results.

capacitive coupling, therefore no simulations can be run under 100 W and mode transitions will not be observed. For input powers higher than 100 W, the model agrees qualitatively well with the experimental results; however, it predicts densities that are nearly 5 times higher for chlorine mixtures. The agreement is better for pure Ar discharge, where n_e is overestimated by a factor 3. This overestimation may have several origins. Firstly, the chemistry database for mixtures of Cl_2 and Ar may require additional work in terms of reaction cross sections and rate constants. The current set of inelastic processes included in the model may underestimate the energy loss for electrons. Secondly, we believe that the drift–diffusion approximation is not well adapted to the pressure range studied in this paper. At high pressure ($\geqslant$100 mTorr), the ion drift velocity u_i is small compared with the ion thermal velocity v_{thi}, and therefore the

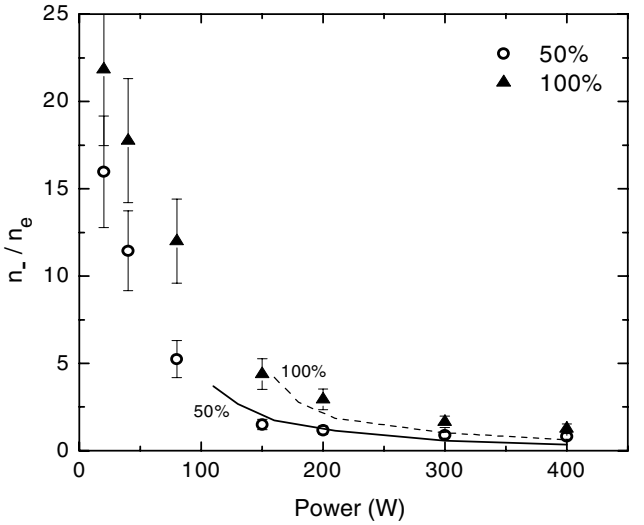

Figure 6. The negative fraction dependence on power at 10 mTorr, for various chlorine concentrations. The dots represent experimental data while lines represent modelling results.

ion neutral collision frequency ν_i is constant. However, for intermediate pressure ranges (1–100 mTorr), a different model is required since the ion mean free path λ_i can approach the characteristic length of the system. Consequently, $u_i \geqslant v_{thi}$ over most of the discharge region and so the ion neutral collision frequency and mobility vary with u_i, introducing a nonlinearity into the ion transport equation [38]. The density profiles are flatter in the middle and steeper at the edge, compared with the cosine profile of the high pressure model. This induces larger positive ion wall losses and could reduce the central ion densities. Thirdly, the measured power transfer efficiency may be overestimated. We should also mention the difficulty of making and interpreting the probe measurements, in particular with a reactive molecular gas like chlorine. Indeed, one must consider that Langmuir probes are an intrusive diagnostic technique which can affect the measured plasma parameters.

The dependence of the negative ion fraction $[n_-]/[n_e]$ with input power for various chlorine concentrations at 10 mTorr is shown in figure 6. At low input powers, the discharge is more electronegative for all mixtures. The electronegativity decreases with increasing input power, which demonstrates, as already reported in oxygen [14], that the inductive mode is less electronegative than the capacitive mode [39]. This is likely due to the increased dissociation of molecular chlorine at high input powers, which are a precursor for negative ion formation. At fixed power, the electronegativity increases with chlorine content, as shown in figures 6 and 11. There is a very good qualitative and quantitative agreement between the experiment and the simulation. However, one should remember that the quantitative agreement rests on the fact that both n_e and n_- are overestimated by a factor 5, as discussed previously.

4.2. Pressure dependence

This section discusses the pressure dependence of the electron density and negative ion fraction. Referring to figure 7,

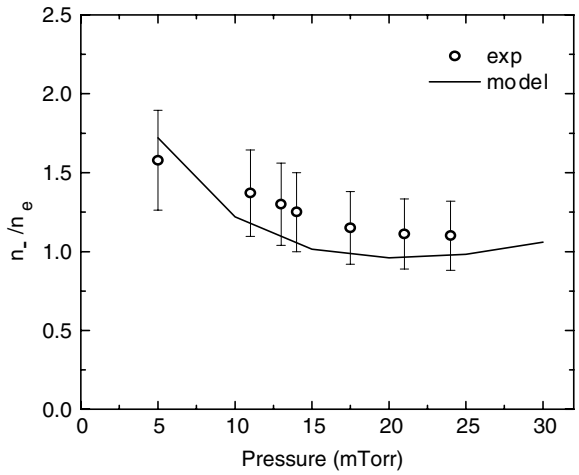

Figure 7. The negative fraction dependence on pressure at 200 W, for a 1 : 1 argon–chlorine plasma. The dots represent experimental data while the line represents modelling results.

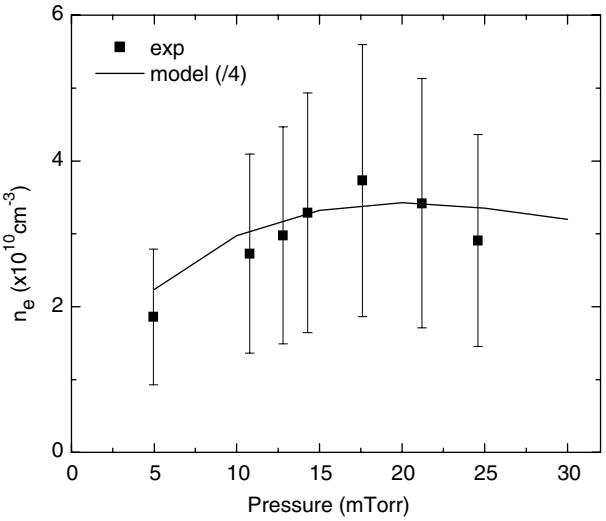

Figure 8. The electron density dependence on pressure at 200 W, for a 1 : 1 argon–chlorine plasma. The dots represent experimental data while the line represents modelling results.

the measured negative ion fraction decreases with increased pressure from 1.6 at 5 mTorr to 1.1 at 25 mTorr. These measurements were taken for a 1 : 1 argon–chlorine plasma operating at 200 W input power. The negative ion fraction predicted by the model is in good agreement with the experiment, both qualitatively and quantitatively. The pressure dependence of the electron density is shown in figure 8. The measured density displays a maximum near 17 mTorr at $3.7 \times 10^{10}\,\mathrm{cm}^{-3}$. A similar dependence was observed by Khater and Overzet [40] when operating with a pure chlorine discharge. They observed that this dependence on pressure varies at different axial positions. Close to the power deposition region (i.e. near the quartz window), the electron and ion densities increase with increasing pressure and then saturate or even decrease, while close to the lower electrode (i.e. near the wafer), the densities decrease monotonically with increasing pressure. The model clearly displays this dependence on axial position. Figures 9 and 10 show how the spatial distribution of electrons and negative

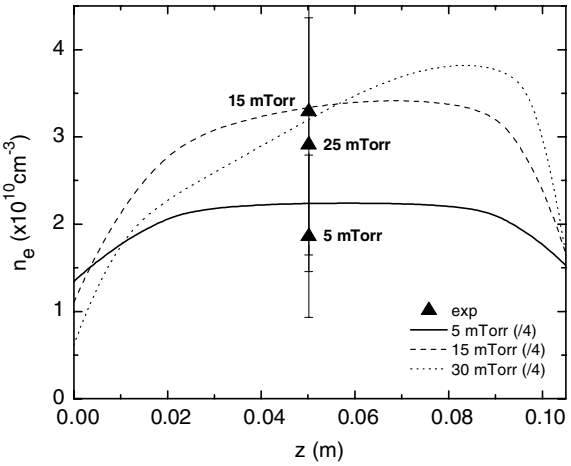

Figure 9. The electron density dependence on axial position z at 200 W, for a 1 : 1 argon–chlorine plasma. The dots represent experimental data while lines represent modelling results, for different values of pressure. Note that in this plot, the densities predicted by the model (lines) have been reduced by a factor of 4.

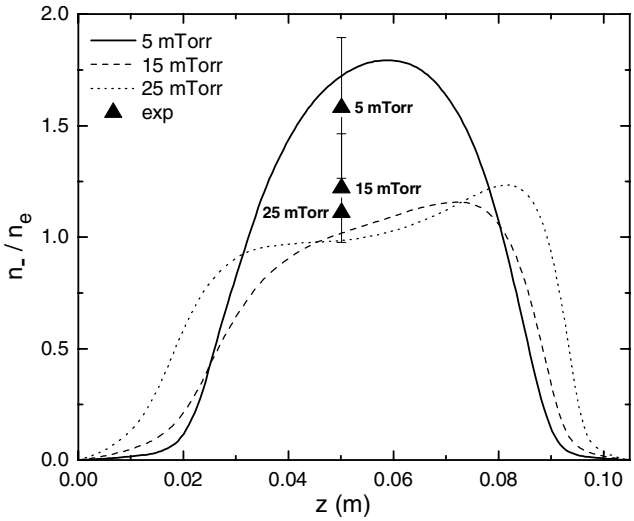

Figure 10. The negative ion fraction dependence on axial position z at 200 W, for a 1 : 1 argon–chlorine plasma. The dots represent experimental data while lines represent modelling results, for different values of pressure.

ions changes with pressure. With increasing pressure, we observe that power absorption and distribution of electrons become more localized below the quartz window, as previously reported [40]. It should also be noted that several other processes might occur when changing the pressure. For instance, the transition from the capacitive to the inductive mode may occur at different input powers for specified pressures. Hence by remaining at a fixed power and by varying the pressure (as we have performed in the experiment), the discharge may switch between capacitive and inductive modes.

4.3. Ar/Cl_2 ratio

The dependence of the negative ion fraction on argon–chlorine mixtures is shown in figure 11. The measurements were

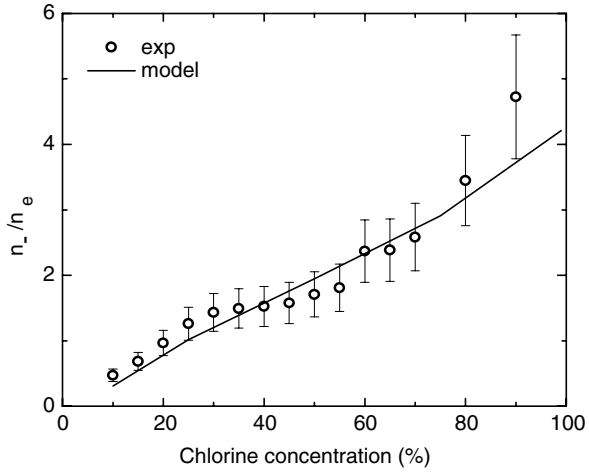

Figure 11. The negative fraction dependence on chlorine concentration at 200 W and 10 mTorr. The dots represent experimental data while the line represents modelling results.

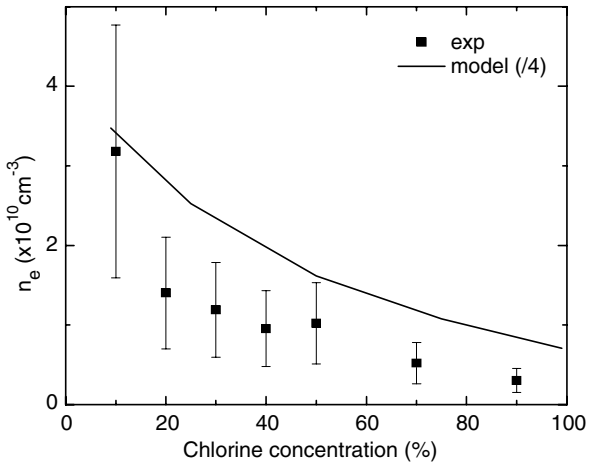

Figure 12. The electron density dependence on chlorine concentration at 200 W and 10 mTorr. The dots represent experimental data while the line represents modelling results. Note that in this plot, the density predicted by the model (line) has been reduced by a factor of 4.

taken with no systematic order in order to avoid any long time-scale effects (e.g. measurements were made with 10% of Cl_2, then 70%, then 35%, etc). The negative ion fraction increases from 0.3 with 10% of Cl_2 to nearly 5 with 90% of Cl_2, but not linearly. This increase is most rapid with increasing chlorine concentration up to 30% and then slows down. Between chlorine concentrations of 30% and 55%, the plasma appears to be depleted of negative ions as the negative ion fraction remains fairly uniform with a value around 1.5. Again there is good qualitative agreement between the experiment and the model (line). However, the model does not display any 'concentration window' where the negative ion fraction remains fairly uniform.

The dependence of the electron density on chlorine concentration is shown in figure 12. As expected, the measured electron density decreases with increasing chlorine content due to energy loss in molecular gases. The electron density decreased rapidly from $7.5 \times 10^{10}\,\mathrm{cm}^{-3}$ in pure argon to $1.4 \times 10^{10}\,\mathrm{cm}^{-3}$ with 20% chlorine. For chlorine concentrations greater than 20%, the decrease in the electron density is more gradual. In figure 12, the density predicted by the model (line) has been reduced by a factor of 4 but the trend agrees well with the experiment.

5. Conclusion

In this paper, we describe results from experiment and simulations of Ar/Cl_2 and Cl_2 plasmas in a low-pressure inductively coupled reactor. The major goal of this work was to make a systematic and detailed comparison between experimental data and model predictions under a wide range of operating conditions, which is essential for plasma processing and validation of models.

Simulations show that the wall recombination coefficient of Cl atom is a crucial parameter of the model and that plasma densities, especially neutral densities, are very sensitive to its variations. By modifying the recombination coefficient, not only do we quantitatively change the densities but we also obtain different evolution trends with pressure or chlorine content. The best agreement between the model and the experiment is obtained for $\gamma = 0.02$, a much lower value than predicted by theory for stainless steel walls (0.6).

In Cl_2-rich conditions and above 150 W, the EEPF appears to be nearly Maxwellian, therefore our Maxwell–Boltzmann treatment of electrons in the model is a good approximation for Ar/Cl_2 mixtures in inductive mode. By increasing power, the discharge switches from the capacitive to the inductive mode and the plasma electronegativity decreases strongly. At high pressure, the power absorption and the distribution of charged particles become more localized below the quartz window, as previously reported.

In general, changes in trends and profiles obtained in the simulation are in close agreement with the experiments. However, the calculated charged particle densities are systematically overestimated by a factor of 3–5. This overestimation may have several origins. Firstly, the chemistry database for mixtures of Cl_2 and Ar may require additional work in terms of reaction cross sections and rate constants. Indeed, the current set of inelastic processes included in the model may underestimate the energy loss for electrons. We also believe that the drift–diffusion approximation is not well adapted to the pressure range studied in this paper. Indeed, for our intermediate pressure range (1–50 mTorr), a different model is required since the ion mobility varies with the ion drift velocity, introducing a nonlinearity into the ion transport equation. This induces larger densities at the edges and consequently larger positive ion wall losses, which could reduce the central ion densities. Also, the measured power transfer efficiency may be overestimated. Finally, one must consider that Langmuir probes are an intrusive diagnostic technique which can affect the measured plasma parameters. A non-intrusive measurement of the plasma density by Thomson scattering or microwave interferometry would serve as a useful comparison to verify the present experimental data.

Acknowledgment

This work was financially supported by the Thales Group.

References

[1] Guilet S, Bouchoule S, Jany C, Corr C S and Chabert P 2006 *J. Vac. Sci. Technol.* B **24** 2381
[2] Hsueh K, Hsu H, Wang C, Huang S and Hsin Y 2005 *Appl. Phys. Lett.* **87** 252107
[3] Shul R J, McClellan G B, Broggs R D, Rieger D J, Pearton S J, Abernathy C R, Lee J W, Constantine C and Barratt C 1997 *J. Vac. Sci. Technol.* A **15** 633
[4] Hahn Y B, Hays D C, Donovan S M, Abernathy C R, Han J, Shul R J, Cho H, Jung K B and Pearton S J 1999 *J. Vac. Sci. Technol.* A **17** 768
[5] Lieberman M A and Lichtenberg A J 1994 *Principles of Plasma Discharges and Materials Processing* (New York: Wiley)
[6] Tuszewski M 1996 *J. Appl. Phys.* **79** 8967
[7] Lieberman M A, Lichtenberg A J and Marakhtanov A M 1999 *Appl. Phys. Lett.* **75** 3617
[8] Chabert P, Lichtenberg A J, Lieberman M A and Marakhtanov A M 2001 *Plasma Sources Sci. Technol.* **10** 478
[9] Chabert P, Lichtenberg A J, Lieberman M A and Marakhtanov A M 2003 *J. Appl. Phys.* **94** 831
[10] Chabert P, Abada H, Booth J P and Lieberman M A 2003 *J. Appl. Phys.* **94** 76
[11] Tuszewski M, White R R and Wurden G A 2003 *Plasma Sources Sci. Technol.* **12** 396
[12] Tuszewski M and White R R 2003 *J. Appl. Phys.* **94** 2858
[13] Goodman D L and Benjamin N 2003 *J. Phys. D: Appl. Phys.* **36** 2845
[14] Corr C S, Steen P G and Graham W G 2003 *Plasma Sources Sci. Technol.* **12** 265
[15] Corr C S, Steen P G and Graham W G 2005 *Appl. Phys. Lett.* **86** 141503
[16] Tinch S, Boullart W and Bogaerts A 2008 *J. Phys. D: Appl. Phys.* **41** 065207
[17] Efremov A M, Dong-Pyo K and Chang-Il K 2005 *Thin Solid Films* **471** 328
[18] Efremov A M, Dong-Pyo K and Chang-Il K 2004 *Plasma Sci. IEEE Trans.* **32** 1344
[19] Efremov A M, Dong-Pyo K and Chang-Il K 2003 *J. Vac. Sci. Technol.* A **21** 1568
[20] Marro F G and Graham W G 2008 *Plasma Sources Sci. Technol.* **17** 015007
[21] Cantin A and Gagne R R 1977 *Appl. Phys. Lett.* **30** 316
[22] Mahony C M O, McFarland J, Steen P G and Graham W G 1999 *Appl. Phys. Lett.* **75** 331
[23] Druyvesteyn M J 1930 *Z. Phys.* **64** 781
[24] Hopkins M B and Graham W G 1986 *Rev. Sci. Instrum.* **57** 2210
[25] Bacal M, Hamilton G W, Bruneteau A M and Doucet J 1979 *Rev. Sci. Instrum.* **50** 719
[26] Bacal M and Hamilton G W 1979 *Phys. Rev. Lett.* **42** 1538
[27] Rosenstock H M, Draxl K, Steiner B W and Herron J T 1977 *Energetics of Gaseous Ions J. Phys. Chem. Ref. Data* **6** (Suppl. 1)
[28] Gottscho R A and Gaebe C E 1986 *IEEE Trans. Plasma Sci.* **PS-14** 92
[29] Fleddermann C B and Hebner G A 1997 *J. Vac. Sci. Technol.* A **15** 1955
[30] Ono K, Oomori T, Tuda M and Namba K 1992 *J. Vac. Sci. Technol.* A **10** 1071
[31] Hsu C C, Nierode M A, Coburn J W and Graves D B 2006 *J. Phys. D: Appl. Phys.* **39** 3272
[32] Bukwski J D, Graves D B and Vitello P 1996 *J. Appl. Phys.* **80** 2614
[33] Lee C and Lieberman M A 1995 *J. Vac. Sci. Technol.* A **13** 368
[34] Christophorou L G and Olthoff J K 1999 *J. Phys. Chem. Ref. Data* **28** 131
[35] Rogoff G L, Kramer J M and Piejak R B 1986 *IEEE Trans. Plasma Sci.* **14** 103
[36] Kota G P, Coburn J W and Graves D B 1998 *J. Vac. Sci. Technol.* A **16** 270
[37] Cunge G, Sadeghi N and Ramos R 2007 *J. Appl. Phys.* **102** 093304
[38] Godyak V A 1986 *Soviet Radiofrequency Discharge Research* (Fall Church, VA: Delphic Associates)
[39] Malyshev M V and Donnelly V M 2001 *J. Appl. Phys.* **90** 1130
[40] Khater M H and Overzet L J 2004 *Plasma Sources Sci. Technol.* **13** 466